iScience

CellPress
OPEN ACCESS

Article

Green oxygen power plants in the brain rescue neuronal activity

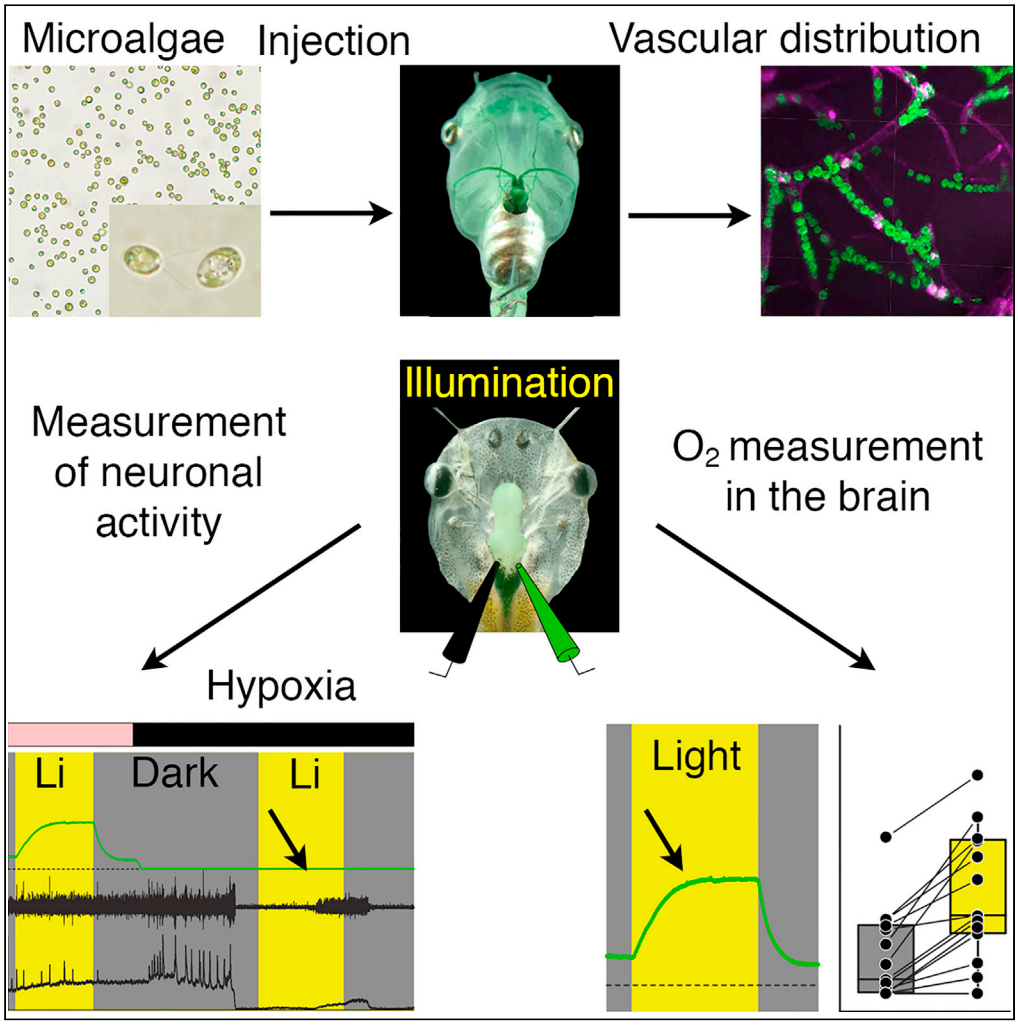

Suzan Özugur, Myra N. Chávez, Rosario Sanchez-Gonzalez, Lars Kunz, Jörg Nickelsen, Hans Straka

straka@lmu.de

Highlights

Transcardially injected microalgae accumulate in brain blood vessels of *Xenopus*

Upon illumination, green algae and cyanobacteria robustly produce O_2 in the brain

After hypoxic loss of brain function, photosynthetic oxygen rescues neural activity

Özugur et al., iScience *24*, 103158
October 22, 2021
https://doi.org/10.1016/j.isci.2021.103158

iScience

CellPress
OPEN ACCESS

Article

Green oxygen power plants in the brain rescue neuronal activity

Suzan Özugur,[1,2] Myra N. Chávez,[3,5] Rosario Sanchez-Gonzalez,[1] Lars Kunz,[1] Jörg Nickelsen,[3] and Hans Straka[1,4,*]

SUMMARY

Neuronal activity in the brain depends on mostly aerobic generation of energy equivalents and thus on a constant O_2 supply. Oxygenation of the vertebrate brain has been optimized during evolution by species-specific uptake and transport of O_2 that originally derives from the phototrophic activity of prokaryotic and eukaryotic organisms in the environment. Here, we employed a concept that exploits transcardial injection and vascular distribution of unicellular green algae or cyanobacteria in the brain of *Xenopus laevis* tadpoles. Using oxygen measurements in the brain ventricle, we found that these microorganisms robustly produce sizable amounts of O_2 upon illumination. In a severe hypoxic environment, when neuronal activity has completely ceased, the photosynthetic O_2 reliably provoked a restart and rescue of neuronal activity. In the future, phototrophic microorganisms might provide a novel means to directly increase oxygen levels in the brain in a controlled manner under particular eco-physiological conditions or following pathological impairments.

INTRODUCTION

Oxygen is a highly important molecule in the energy production cascade, required for metabolic processes, as well as for differentiation and growth of cells and tissues (Carreau et al., 2011; Fathollahipour et al., 2018). In vertebrates including humans, O_2 is taken up *via* respiration mainly by lungs, gills and skin (Piiper, 1982; Sacca and Burggren, 1982; West, 2018) and reaches all regions of the body through a structurally conserved vascular system (Crystal and Pagel, 2020). The brain in particular requires a considerable and constant supply of O_2 to provide the energy for undisturbed neuronal computations for e.g., sensory-motor processing and cognitive functions (Ames, 2000; Schneider et al., 2019). Although oxygenation of the vertebrate brain has been optimized during evolution, specific eco-physiological conditions such as deep-sea diving or flying at high altitudes challenge an adequate O_2 supply of the tissue (Hoiland et al., 2018; Kooyman et al., 2020). In addition, pathologically abnormal hypoxic conditions because of strokes or when O_2 extraction from the environment is compromised can severely and irreversibly deteriorate brain function.

Detrimental effects of hypoxia can be ameliorated by enhanced O_2 levels through species-specific uptake and delivery mechanisms, culminating in techniques such as the hyperbaric oxygenation therapy for human patients (Poli and Veltkamp, 2009). The strict dependency of animals on environmental O_2 is in contrast to green plants, which are able to self-produce O_2 in light through photosynthesis (Martin et al., 2018). Provided photosynthetic microorganisms such as algae and cyanobacteria can be inserted and distributed throughout the tissue such as the brain, their O_2-producing ability might directly supplement the respective needs of animals. In fact, natural symbiotic interactions between such microorganisms and animals are reported for members of the phyla *Porifera* (sponges), *Cnidaria* (corals, sea anemones; Venn et al., 2008) and also salamander species (Burns et al., 2020; Kerney et al., 2011). By mimicking this natural principle, microalgae have occasionally been employed in biomedical science as efficient O_2 source, mostly to supplant absent blood perfusion of isolated tissue (Chávez et al., 2020). This culminated in a tissue-engineered co-culture of the microalga *Chlamydomonas reinhardtii* and fibroblasts to form a dermal scaffold that facilitates healing of skin wounds in mice through photosynthetic O_2 production (Hopfner et al., 2014) or in the case of *Synechococcus elongatus* in a photon-powered myocardium of the ischemic heart (Cohen et al., 2017).

[1]Department Biology II, Ludwig-Maximilians-University Munich, Großhaderner Str. 2, 82152 Planegg, Germany

[2]Graduate School of Systemic Neurosciences, Ludwig-Maximilians-University Munich, Großhaderner Str. 2, 82152 Planegg, Germany

[3]Department Biology I, Ludwig-Maximilians-University Munich, Großhaderner Str. 4, 82152 Planegg, Germany

[4]Lead contact

[5]Present address: Institute of Anatomy, University of Bern, Bern, Switzerland

*Correspondence: straka@lmu.de

https://doi.org/10.1016/j.isci.2021.103158

The pronounced O_2 dependency of neuronal activity prompted us to explore an innovative concept of photosynthetic O_2 replenishment of the brain. Following transcardial injection of green algae or cyanobacteria and their vascular distribution in *Xenopus* tadpoles, illumination of the brain triggered a robust and constant production of oxygen. Moreover, in an artificially generated, severe hypoxic environment, which completely abolished neuronal activity, light-induced O_2 production by the microorganisms caused a restart of the neuronal spike discharge and thus rescued brain activity. These proof-of-principle experiments clearly demonstrate the possibility to utilize O_2-producing phototrophic microorganisms inside a vertebrate brain to directly provide the brain and its cells with O_2. This has the potential consequence that extraction of environmental O_2 becomes at best unnecessary. In the future, this might provide a novel means to increase O_2 levels in the tissue in a temporally and spatially controlled manner under particular eco-physiological conditions or following pathological impairments.

RESULTS

Photosynthetic O_2 production by *C. reinhardtii* and *Synechocystis* sp. PCC6803

The capacity of photosynthetic O_2 production was determined in suspensions of 10^8 cells/mL for wild-type and photomutant strains of the prokaryotic cyanobacterium *Synechocystis* sp. PCC6803 (denominated hereafter *Synechocystis* 6803) and the eukaryotic microalga *C. reinhardtii* representing the most commonly used prokaryotic and eukaryotic unicellular model organisms in photosynthesis research, respectively (Figures 1A–1C). Illumination at an intensity of 5400 lux (Zeiss CL 6000 LED with >150 W) raised the O_2 concentration in the tube to similar levels for wild-type *C. reinhardtii* (2267 $\pm$ 310 μmol/L; mean $\pm$ sem) and *Synechocystis* 6803 (2244 $\pm$ 161 μmol/L; mean $\pm$ sem). In contrast, illumination of the respective photomutants (see STAR Methods) caused a reduction of the O_2 levels in suspensions of both *C. reinhardtii* (-292 ± 10 μmol/L) and *Synechocystis* 6803 (-171 ± 19 μmol/L), indicative of respiratory O_2 consumption (Figure 1C). Suspensions were injected in separate sets of experiments into the vascular system of *Xenopus* tadpoles to test the capacity of generating O_2 inside brain blood vessels.

Distribution of microorganisms in the vascular system

A volume of 10 μL of *C. reinhardtii* or *Synechocystis* 6803, suspended in frog Ringer (both 10^{10} cells/mL) was pressure-injected through a glass capillary in pulses of ~0.2 μL into the tadpole heart under deep MS-222 anesthesia (Figure 1D). The pulses were synchronized with the heartbeat to facilitate contraction-timed release into the aortic arches (Video S1). The progressive vascular dispersion of the microorganisms became visible by the green staining of blood vessels in e.g., the skin that gradually intensified over the injection period (Figures 1E and 1F). Successful transport into brain blood vessels was confirmed by co-injecting Isolectin, a fluorescent molecule that binds to the vascular endothelium (Figures 1G–1J and S1). Confocal z stack reconstructions of whole mount brains revealed the vascular structure (magenta in Figures 1G, 1H and S1) and colocalized autofluorescence of chlorophyll in *C. reinhardtii* and *Synechocystis* 6803 cells (green in Figures 1G and 1H). Higher magnifications and optical re-sectioning of the tissue in the hindbrain region revealed individual microorganisms inside the blood vessels (Figures S1B1–S1B3 and S1C). While smaller *Synechocystis* 6803 cells were generally more densely packed in most vessels (Figure 1J), larger *C. reinhardtii* cells usually formed a pearl chain-like arrangement (Figure 1I). The high density of either species inside brain blood vessels provides an excellent prerequisite for efficient photosynthetic O_2 production.

Photosynthetic O_2 production in the brain

The capacity of photosynthetic O_2 production by *C. reinhardtii* and *Synechocystis* 6803 in the brain was evaluated in semi-intact preparations of *Xenopus laevis* tadpoles (Figure 2A). Such preparations have been well-established for various studies of neuronal computations (Straka and Simmers, 2012) including monitoring of O_2 dynamics in the brain (Özugur et al., 2020). The intact peripheral and central nervous systems of these preparations allow extended physiological recordings of activity profiles that are comparable to those in intact animals (Straka and Simmers, 2012). Following injection of the microorganisms into the vascular system and subsequent isolation of the tissue, preparations were superfused with frog Ringer that either contained air-saturated ($[O_2] = 263 \pm 6$ μmol/L; $N = 14$) or carbogen-elevated O_2 levels in the bath ($[O_2] = 761 \pm 27$ μmol/L; mean $\pm$ sem; $N = 50$). The corresponding O_2 level in the brain was monitored by an additional O_2 electrode within the IVth ventricle (Figure 2A), a position known to directly reflect the O_2 concentration of the adjacent brain region, whereas the spike discharge of the *superior oblique* motor nerve served as proxy for brain activity (Özugur et al., 2020).

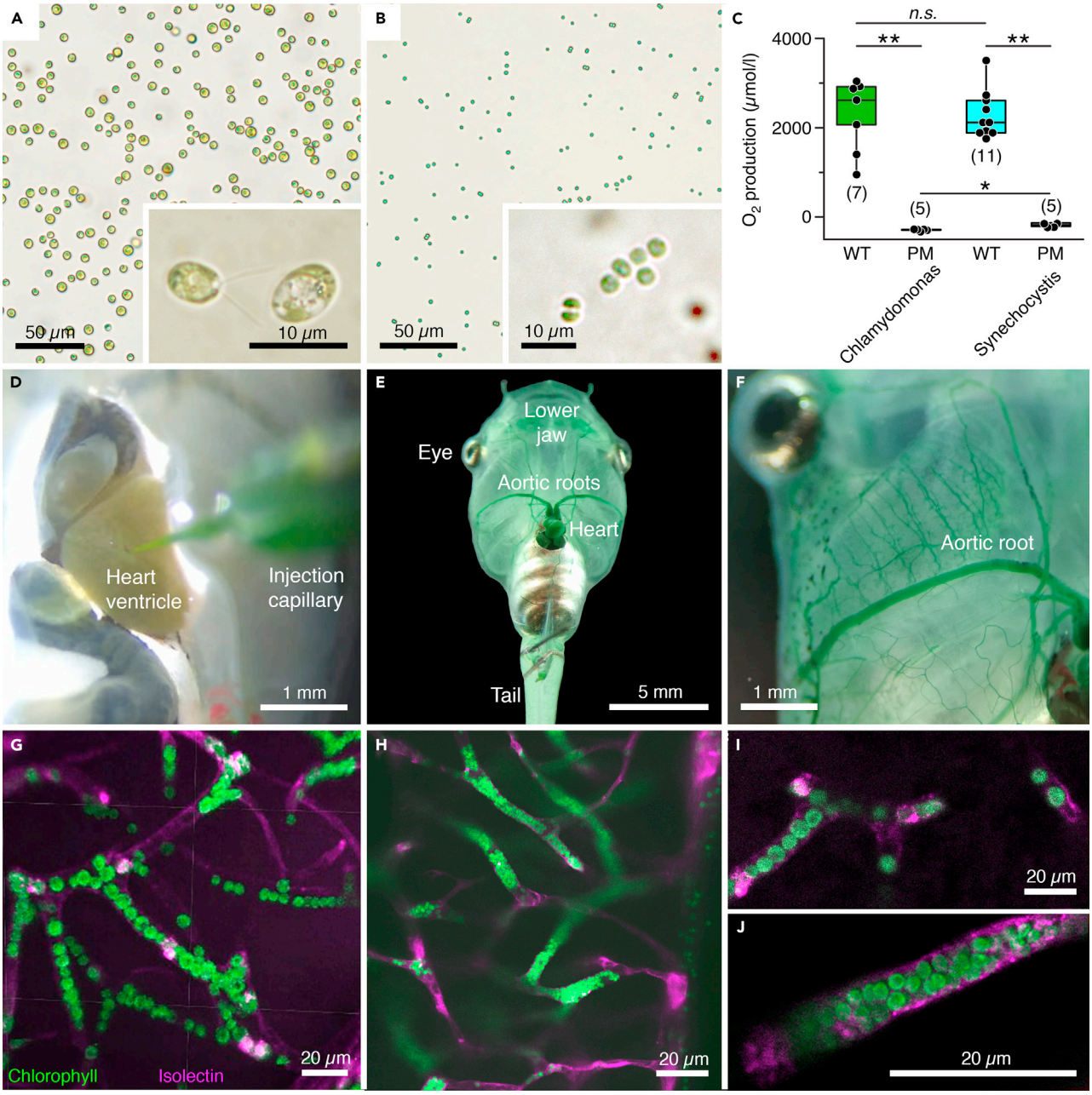

Figure 1. Transcardial injection and accumulation of photosynthetic microorganisms in blood vessels of *Xenopus laevis* tadpoles

(A and B) Microphotographs depicting *C. reinhardtii* (A) and *Synechocystis* 6803 (B) before injection; insets show the microorganisms at higher magnification.

(C) Light-induced O_2 production and lack thereof, respectively, in solutions (10^8 cells/mL) of wild-type (WT) and photomutant (PM) strains of the two species; number of experiments indicated in parentheses.

(D–F) Photographs depicting pressure-injection of a *Synechocystis* 6803 solution into the heart (D) and distribution of the microorganisms through the aortic roots (E,F) and smaller blood vessels (green staining) of the body (E) and lower jaw (F).

(G–J) Confocal reconstruction of hindbrain tissue, illustrating accumulated *C. reinhardtii* (G and I) and *Synechocystis* 6803 (H and J) inside blood vessels; microorganisms appear in green due to chlorophyll autofluorescence and blood vessels in magenta by isolectin-stained endothelial walls. Calibration bars represent 50 μm (A and B), 10 μm (insets), and 1 mm (D and F), 5 mm (E), 20 μm (G–J). *, $p < 0.05$; **, $p < 0.01$; Mann Whitney U-test, Bonferroni-corrected; *n.s.* not significant.

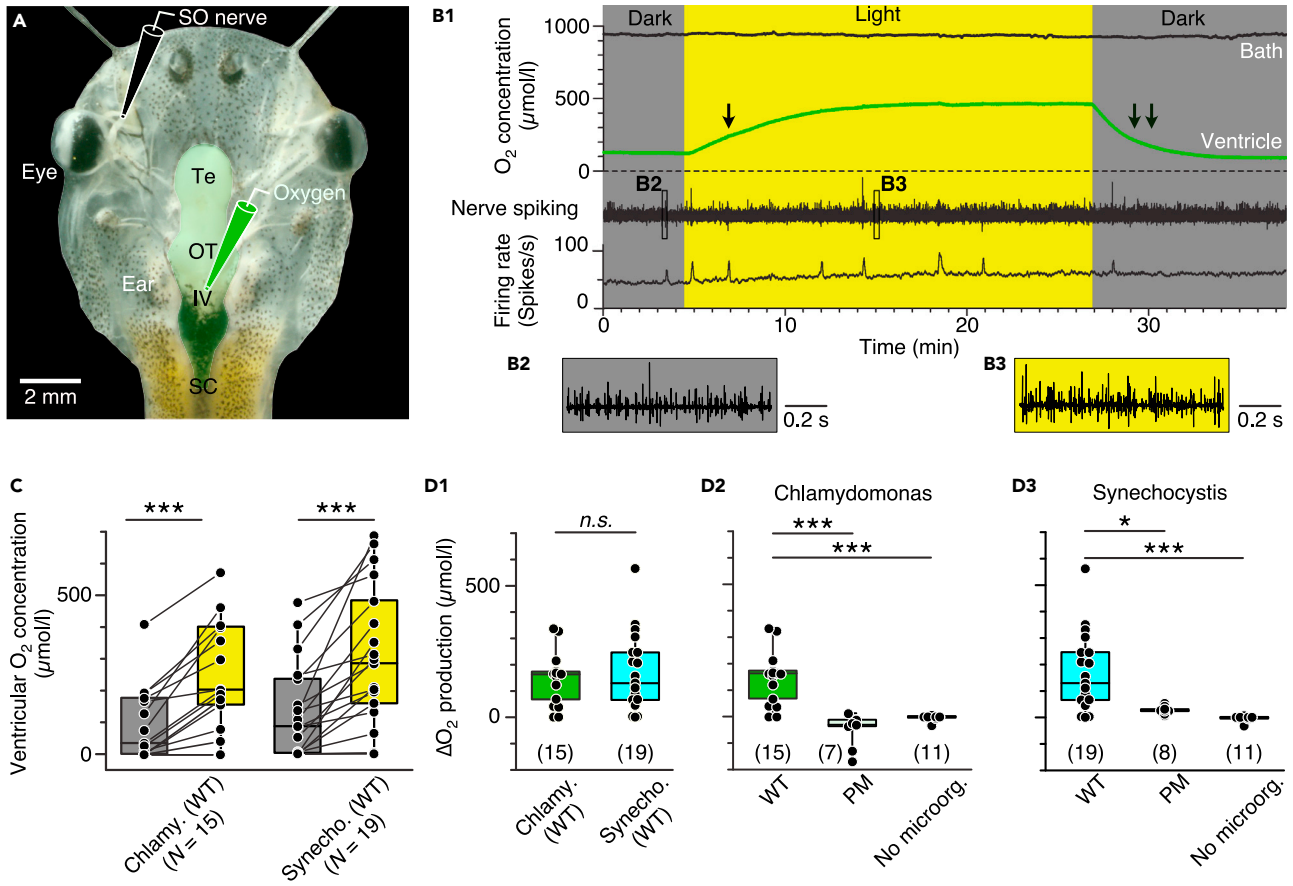

Figure 2. Photosynthetic oxygen production in the brain

(A) Semi-intact head preparation, illustrating the recording of O_2 concentrations in the IVth ventricle (green electrode) and of *superior oblique* (SO) nerve spike discharge (black electrode).

(B) Episode (B1) of O_2 concentration recording in the bath chamber (black trace) and IVth ventricle (green trace) and of concurrent multi-unit SO nerve spiking and mean firing rate (black trace) in darkness and light in a preparation containing *C. reinhardtii*; the ventricular O_2 concentration increases during illumination with a slower rise (single arrow) and faster decay (double arrow); insets depict SO nerve spiking in darkness (B2) and light (B3) at higher temporal resolution.

(C) Boxplot depicting ventricular O_2 concentrations in darkness (gray bars) and light (yellow bars) in preparations containing wild-types of *C. reinhardtii* or *Synechocystis* 6803; ***, $p < 0.001$, Wilcoxon signed-rank test.

(D) Boxplots depicting light-induced changes (Δ) of O_2 concentrations in preparations containing either wild-type (WT) microorganisms (D1) in comparison with photomutant (PM) strains or controls without *C. reinhardtii* (D2) or *Synechocystis* 6803 (D3); number of experiments indicated in parentheses. *, $p < 0.05$, ***, $p < 0.001$, Mann Whitney U-test, Bonferroni-corrected; *n.s.* not significant.

Illumination of semi-intact preparations containing wild-type microorganisms caused an asymptotic increase of the brain O_2 concentration that remained at an elevated level until the light was switched off, which caused a gradual return to control O_2 levels in darkness (green trace in Figure 2B1). In contrast to the ventricle, the bath O_2 concentration was light-insensitive (black trace in Figure 2B1). The photosynthetic O_2 production in the brain was robust and reliably inducible in the vast majority of preparations containing either *C. reinhardtii* (N = 13 out of 15) or *Synechocystis* 6803 (N = 16 out of 19) with individual values occasionally exceeding 500 µmol/L (Figures 2C and 2D). Although both species of microorganisms increased the O_2 concentration to similar extents (~150 µmol/L; Figure 2D1), production onset and rise time to reach a steady-state plateau were faster for *Synechocystis* 6803 than for *C. reinhardtii* (Figures S2A and S2B). The decay times upon light extinction (double arrow in Figure 2B1) were comparable for both microorganism species but significantly faster than the respective rise times (single arrow in Figure 2B1 and S2C). This suggests that the decay largely reflects the O_2 consumption dynamics of the brain tissue (Özugur et al., 2020) once photosynthetic O_2 production has ceased.

Illumination without prior injection of microorganisms consistently failed to increase the ventricular O_2 concentration (Figures 2D, S2D (red trace), and S2F), demonstrating that the increase in O_2 concentration in the

presence of wild-type *C. reinhardtii* or *Synechocystis* 6803 (Figures 2B–2D) was not because of an unspecific photo-effect but of photosynthetic origin. This was further corroborated by employing photomutant strains of the two species each lacking the O_2-producing photosystem II complex (Figures 1C, 2D, S2E, and S2G). Illumination of *Xenopus* tadpole preparations containing such photomutants either increased the ventricular O_2 level only marginally (*Synechocystis* 6803) or even reduced the overall O_2 level (*C. reinhardtii*; Figures S2E and S2G). Altogether, these experiments confirm the specificity of the photosynthetic enhancement of ventricular O_2 levels by unicellular microalga/cyanobacteria.

Correspondence between O_2 levels and neuronal activity

Recordings of multi-unit spike discharge of the *superior oblique* nerve revealed a clear correlation between spike firing rate and ventricular O_2 level (Figure 2B). The firing rate significantly increased following augmentation of the ventricular O_2 level from 0 μmol/L at air-saturated bath O_2 levels to ~180 μmol/L (183 ± 45 μmol/L; N = 12) by simple ventilation of the bath Ringer with carbogen (Figure S3A). A comparable firing rate increase was achieved by illumination when either wild-type *C. reinhardtii* (Figure 2B) or *Synechocystis* 6803 were present in the brain (Figures S3B and S3E). This enhancement was specific because illumination of preparations without microorganisms or with photomutants left the *superior oblique* nerve activity as well as the ventricular O_2 level unaltered (Figures S3C, S3D, S3E2, and S3E3). Collectively, the outcome of the different experimental conditions therefore indicates that the discharge rate correlates with the ventricular O_2 level (Figure S3F). The link between ventricular O_2 level and neuronal activity was further validated during spontaneous spike bursts in the *superior oblique* nerve (Figure S3G1). Such episodes of enhanced neuronal activity are usually accompanied by an augmented O_2 demand, previously demonstrated as a transient reduction of the ventricular O_2 level (Özugur et al., 2020). During photosynthetic O_2 production, such spike burst-related increases in O_2 demand became apparent as burst-timed, transient reduction of the ventricular O_2 concentration (▼ in Figures S3G1 and S3G2), providing evidence that the O_2 generated by photosynthesis effectively supports enhanced neuronal activity.

Rescue of neuronal activity by photosynthetic O_2 production

Direct proof for photosynthetic O_2 supply in the absence of other O_2 sources is presented in a final set of experiments. Removal of most O_2 from the bath Ringer solution to a level <40 μmol/L by continuous ventilation with N_2 completely abolished the spike discharge of the *superior oblique* nerve. This loss occurred in darkness within ~20 min (white arrow heads in Figure 3A1) independent of the presence or absence of microorganisms (Figure 3B). Subsequent illumination of the preparation in the presence of wild-type *Chlamydomonas* or *Synechocystis* in brain blood vessels provoked a restart of the spike activity (black arrow heads in Figures 3A1 and A4) with a latency of 15–20 min (Figure 3C). This was faster compared to the restart of spike discharge by ventilation of the bath Ringer solution with carbogen (~40 min).

Repetitive periodic alterations of darkness and illumination during continuous ventilation of the bath solution with N_2, to maintain low O_2 bath levels, caused the *superior oblique* nerve spike discharge to reversibly cease in darkness (white arrow heads in Figure 3A1) and to restart soon after illumination onset (black arrow heads in Figure 3A1). Following light-induced restart of the discharge, the firing rate gradually increased and reached the same level (*C. reinhardtii*, Figure 3D1) or even exceeded (*Synechocystis* 6803, Figure 3D2) control values at air-saturated Ringer O_2 levels prior to the ventilation with N_2. The re-establishment of neuronal discharge by photosynthetic microorganisms was faster and more effective than ventilation of the bath Ringer with carbogen (Figures 3C and D3), likely because of the direct on-site O_2 production by the microorganisms in the brain, thereby fueling the metabolism for spike generation. Thus, independent of differences in the O_2 production dynamics, *C. reinhardtii* and *Synechocystis* 6803 cells within the brain vascular system produce sufficient amounts of O_2 upon illumination to rescue neuronal spike discharge after O_2 depletion in the environment.

DISCUSSION

Transcardial injection of green algae or cyanobacteria in *Xenopus laevis* tadpoles distributed these photosynthetic microorganisms throughout the CNS causing a light exposure-timed increase of the O_2 concentration upon illumination of the brain. During a general, brain-wide extinction of neuronal activity by sub-atmospheric O_2 levels, green algae, and cyanobacteria were able to reversibly and repetitively

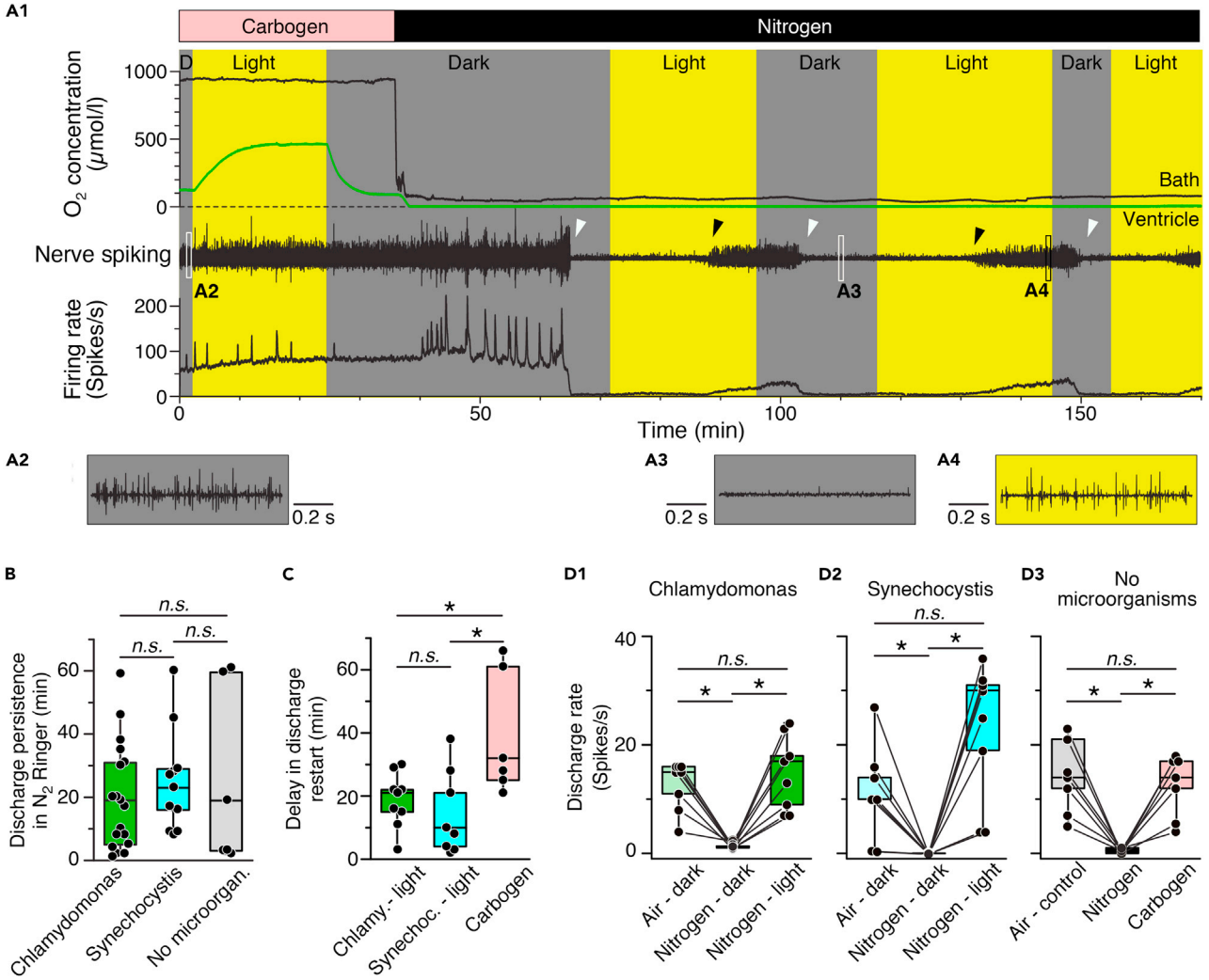

Figure 3. Photosynthetic oxygen production rescues neuronal activity under hypoxic conditions

(A) Episode (A1) of O_2 concentration recording in the bath chamber (black trace) and IVth ventricle (green trace) and of concurrent *superior oblique* nerve spiking and mean firing rate (black trace) at hyperoxic (Carbogen) and hypoxic (Nitrogen) bath O_2 levels during alternating periods of darkness and light in a preparation containing wild-type *Synechocystis* 6803; note that nerve spiking under hypoxic conditions reversibly ceases in darkness (white arrow heads) but can be restarted during illumination (black arrow heads); insets depict nerve spike discharge under control (A2) and hypoxic conditions in darkness (A3) and light (A4) at higher temporal resolution.

(B–D) Boxplots depicting the delay of discharge cessation under hypoxic conditions in darkness (B), light- or carbogen-induced restart of spiking (C) and magnitudes of re-established firing rates (D) with either *C. reinhardtii* (green bars) or *Synechocystis* 6803 (cyan bars) in the vascular system as compared to the firing rate following carbogen-induced restart of spiking (gray/pink bars) in darkness. *, $p < 0.05$, Mann Whitney U-test in (B) and (C), Bonferroni-corrected; Wilcoxon signed-rank test in (D), *n.s.* not significant.

reinitiate the spike activity upon illumination, thereby demonstrating the capacity of these microorganisms to rescue brain activity by photosynthetic O_2.

Injection and distribution of photosynthetic microorganisms

Distribution and accumulation of photosynthetic microorganisms in the brain through the vascular system proofed to be an efficient method to obtain a high concentration of these single-celled organisms in the brain (Figures 1 and S1). This indicates that the cardial pump activity and generated blood flow in *Xenopus* larvae (Video S1) are sufficient to distribute and deposit the microorganisms throughout the entire brain. The invasion of even the finest blood vessels outlined by Isolectin, by both types of microorganisms was confirmed by the reliable and consistent co-staining of the vascular system with Isolectin and the

autofluorescence of the microalgae and cyanobacteria. However, after all a much finer resolution of the imaging system would be required to finally resolve this issue. Although cyanobacteria form densely packed agglomerations even in the smallest vessels, the larger *C. reinhardtii* algae generate pearl-chain aggregations filling the entire volume of the smallest vessels. If this generates a clogging has to be determined in separate sets of experiments. Despite the different intravascular arrangement of the two species, both produced equal amounts of O_2 (Figures 2C and 2D). The magnitude of O_2 production, however, is likely underestimated because the tissue continuously consumes O_2 (Özugur et al., 2020) lowering the detectable amount of O_2 in the ventricular compartment where the measurements were performed. The constantly ongoing consumption of O_2 by the brain tissue in *Xenopus* larvae can reach up to ~700 μmol/L if O_2 levels above air-saturation are available in the Ringer solution (Özugur et al., 2020). This suggests that photosynthetically produced O_2 is likely also fueling the general O_2-dependent metabolic pathways. Even though both species of phototrophic microorganisms were very effective in producing O_2, future studies will have to demonstrate if other microalgae, inertly adapted to colder temperatures (and therefore to typical environments of amphibians), enclosed compartments or extracted from symbiotic interactions might provide even larger amounts of O_2. Such species would therefore allow using lower light levels or specific light spectra and potentially open new avenues for dynamically more efficient on-off switches. Although a brain-wide distribution of the microorganisms through the vascular system is obviously very effective, direct injection of the microorganisms into the ventricular system of the brain of isolated preparations is also possible and might even allow the insertion of larger volumes of algae or cyanobacteria and thus potentially produce higher levels of photosynthetic O_2. However, a ventricular confinement prevents a more localized, site-specific enhancement of O_2 levels through focal illumination of particular brain regions or provides O_2 in areas that are more remotely located with respect to the brain ventricular system.

Photosynthetic oxygen production in isolated preparations

In vitro whole head preparations of *Xenopus* tadpoles are highly suitable for robust measurements of neuronal activity (Straka and Simmers, 2012) or O_2 dynamics in the brain (Özugur et al., 2020). This experimental condition provides a unique setting, in which the O_2 production capacity by green algae or cyanobacteria, contained within brain blood vessels, can be directly explored. In such preparations, the *in vivo*-like setting thereby enabled us to test the capacity of photosynthetic microorganisms to fuel O_2-dependent processes and thus fulfill the energetic needs for neuronal computations. Although these experiments only provided results for the acute stage of O_2 production, the successful demonstration suggests promising applications for which isolated preparations are excellently suited. The possibility to monitor major "vital" parameters of brain function in such preparations, such as synaptic transmission efficacy, spike discharge rates, or burst patterns (Özugur et al., 2020) ensures controlled measurements of neuronal firing and allows manipulations of background O_2 concentrations. At least, in the acute stage, following establishment of the isolated preparation, the injected microorganisms did obviously not deteriorate the viability of the tissue with respect to the magnitude of the neuronal activity (Straka and Simmers, 2012) or O_2 metabolism (Özugur et al., 2020). Given the known toxicity of excessive amounts of O_2, the photosynthetic O_2 production is well within the previously determined optimal range without any impairment of the neuronal activity (Özugur et al., 2020). In fact, higher bath O_2 levels, in the range of the photosynthetic production as evoked in the current study, ameliorated the firing rate of cranial nerves (Özugur et al., 2020), indicating an improvement of the neuronal machinery with elevated O_2 levels. This suggests that phototrophic microorganisms and appropriate illumination have indeed the capacity to improve the quality of neuronal computations in isolated preparations of *Xenopus* larvae but will potentially be also beneficial for other *in vitro* studies of brain activity employing slice preparations or organotypic cell cultures (see below).

In contrast to wild-type microorganisms, photomutants fail to produce O_2, because of the known deficiency in photosystem II (Boudreau et al., 2000; Nixon et al., 1992). The demonstration of this lack of O_2 production has been a major control experiment, because it clearly confirmed that the produced O_2 of the wild-type microorganisms derived from the photosynthetic activity. Although the O_2 production of wild-type microorganisms is in the range of atmospheric O_2 levels, it is unknown if even higher levels are locally present in the vicinity of the blood vessels. Even though, this is possible, it is unlikely that excessively high levels of O_2 are accumulated in the adjacent tissue. In fact, O_2 is very rapidly metabolized up to a level of ~700 μmol/L as demonstrated previously in isolated *Xenopus* preparations (see above; Özugur et al., 2020), generating a safety window for the photosynthetic O_2 production. In addition, given the dependency of the production process on the concentration of the microorganisms, light intensity and spectrum, there are a number of

experimental parameters to fine-tune the amount of O_2 production. Accordingly, it is unlikely that photosynthesis risks an induction of local toxicity because of oxidative damage and the production of reactive oxygen species (Cobley et al., 2018).

Rescue of neuronal activity by photosynthetic oxygen

The key proof-of-principle experiment of the present study was the photosynthetic rescue of neuronal activity during periods of sub-atmospheric O_2 supply, which caused complete cessation of nerve cell spike activity (Figure 3A). The relatively fast abolishment of the spike discharge when reducing the O_2 concentration from an atmospheric level (~270 μmol/L; Özugur et al., 2020) to ~40 μmol/L in the bath Ringer obviously derives from a rapid run-down of energy equivalents, normally produced through aerobic processes (Özugur et al., 2020; Hall et al., 2012). Highly essential to these critical control experiments was the continuous measurement of the O_2 level both in the bath solution as well as in the IV^{th} ventricle as faithful and robust proxy for the concentration in the adjacent hindbrain tissue in the vicinity (Özugur et al., 2020), directly confirming the low level of O_2 in the bath and its absence in the brain (see black and green traces in Figure 3A1). The highly efficient aerobic production of energy equivalents facilitates the energy-costly maintenance of Na^+ and K^+ gradients across the cell membrane as part of spike generation and membrane potential homeostasis (Howarth et al., 2012; Hyder et al., 2013). Obviously, the nervous system, under our hypoxic experimental condition, is unable, too slow or too inefficient to switch to anaerobic energy production to support the neuronal activity. Although low O_2 levels can simply be replenished by supplying oxygenated Ringer solution, photosynthetic microorganisms upon illumination are much faster and more efficient in generating sufficient amounts of O_2 for refueling the aerobic production of energy equivalents required for spike activity (Figures 3C and 3D). In contrast to the slower O_2 increase through the bath solution, the photosynthetic mechanism is more efficient, likely related to the brain-wide distribution of the microorganisms, thereby minimizing the O_2 diffusion distance with respect to the anatomical location of the spike generating neuronal circuits in the hindbrain. Thus, using photosynthetic O_2 production magnitudes as proxy, green algae, and cyanobacteria are highly efficient in fueling aerobic metabolic pathways in animals, in particular in the brain, where the vascular system forms a very dense meshwork (Figure S1A) with short diffusion distances between the vessels and neurons.

Systemic reaction of the immune system upon injection

During the relatively short duration of our experiments (3–4 h) an obvious deterioration of the tissue or the neuronal activity, when microorganisms were present was not observed. However, a major challenge for a future systemic introduction of phototrophic microorganisms, either into the vascular system or directly into the brain ventricular system is the potential activation of an immune response by the host as general reaction to intruders (Medzhitov, 2007). Although such a reaction appears to be inevitable in the case of pathogenic single-celled prokaryotes and eukaryotes, certain microorganisms such as *C. reinhardtii* or *Synechocystis* 6803 might form a favorable exception. For instance, a lack of systemic immune response has been demonstrated when transplanting an algae scaffold onto the skin of mice (Chávez et al., 2020; Schenck et al., 2015). Moreover, injection of these green algae into zebrafish eggs formed chimeras that remained viable for several days and after subsequent extraction from the larvae, the algae continued to grow (Alvarez et al., 2015). This suggests that the period of amalgamation with an animal had no obvious detrimental impact on the fertility of these phototrophic microorganisms in line with natural symbiotic interactions between algae and vertebrates (Burns et al., 2020; Kerney et al., 2011). Moreover, the employment of *Xenopus* tadpoles at mid-larval stages for experiments such as presented here might be advantageous for further exploring the beneficial range of systemically introduced phototrophic microorganisms on brain metabolism and electrical activity because the innate immune system in these animals is only completed after metamorphosis (Godwin and Rosenthal, 2014). Thus, further studies on potential immune responses of the host are required to estimate a potential developmental stage-dependent rejection of the microorganisms and the possibility for long-term survival after chronic insertions.

Potential fields of application

Although biomedical photosymbiosis during tissue engineering has become popular over the past decades (Chávez et al., 2020), the current study considerably advanced the applicability by establishing a novel and innovative concept of O_2 supply in the brain that is able to ameliorate severe outcomes of low ambient O_2 levels with the consequence to rescue neuronal activity. Provided that green algae or cyanobacteria can escape potential immune responses by the host and can steadily produce O_2 upon illumination, the photosynthetic strategy represents a striking and elegant solution to improve pathologies

related to a lack of O_2 in various types of tissues. This opens up several fields of application. Photosynthetic O_2 exploited in empiric experiments could improve the O_2 level in under-perfused tissue, such as cell cultures or brain slices but also explants of lung or kidney. Controllable magnitude, duration and spectrum of the illumination allow a graded O_2 production, opening new avenues for studying the role of O_2 in metabolic processes through fast local production dynamics by focal illumination. Insertion of phototrophic microorganisms into enclosed organs such as the *Xenopus* tadpole inner ear and focal illumination represents an excellent experimental setting that allows testing the functional consequences of bilaterally imbalanced O_2 levels on neuronal computations and motor outputs (Özugur et al., 2020; Lambert et al., 2008). This is based on the fact that enhanced O_2 levels increase the neuronal firing rate (Özugur et al., 2020), likely through more efficient synaptic transmission and/or spike generation mechanisms.

The creation of a symbiosis-like long-term coexistence with a vertebrate after insertion of phototrophic microorganisms might reduce the dependency of an animal on atmospheric O_2, thereby extending the eco-physiological range of respective habitats. The inaccessibility of internal organs of larger and/or non-transparent animals for illumination is circumvented by insertion of green algae or cyanobacteria into the vascular system. Circulating microorganisms can absorb sufficient light when traveling inside blood vessels below the skin and directly provide red blood cells with photosynthetically produced O_2. Although this concept is highly innovative, potentially detrimental aspects such as clogging of blood vessel by the microorganisms or induction of thrombosis must be investigated before chronic intravascular applications. Potential medical areas of photosynthetic O_2 enhancement include tissue infarcts or respiratory impairments that prevent natural extraction of environmental O_2. Although O_2 is the major "byproduct" of the light-reactions of photosynthesis, the subsequent dark reactions finally produce sugars, which when exported from the microorganisms might also supply the host and thus provide a second beneficial byproduct. Apart from such "natural" photosynthetic end products, microorganisms can be genetically engineered to produce various releasable substances such as, e.g., the vascular endothelial growth factor VEGF (Chávez et al., 2016). This factor has been demonstrated to induce the formation of blood vessels in the host tissue when released from the algae, transplanted onto the skin of mice (Chávez et al., 2016). Thus, the generation of chimeras between vertebrates and photosynthetic microorganisms might reveal a number of basic principles of O_2 metabolism but even more importantly open new approaches and avenues for a variety of applications that currently still fall into the realm of science fiction.

Limitations of the study

Following transcardial injection of the desired volume, it is very probable that only an unknown fraction of the microalgal suspension were distributed throughout the vascular system including brain blood vessels, because part of the microalgae accumulated in the atrium of the heart. Despite the consistent co-labeling blood vessels and microalgae, high-resolution imaging studies will have to demonstrate the lower limits of the invasion of the smallest brain blood vessels by both types of unicellular algae. The measurement of the oxygen concentration upon illumination yielded robust and reliable increases; however, the obtained maximal levels might have been even underestimated, given the rapid turnover of O_2 by cells in the brain, once oxygen becomes available in the tissue. While neuronal activity was ongoing for several hours, indicating functional integrity of the isolated preparation, it is currently unknown how much oxidative stress is created by repetitive illumination of the microorganisms and the photosynthetic production of O_2. Based on the known survival of such preparations for days, longer-term experiments will have to determine the applicability range.

STAR★METHODS

Detailed methods are provided in the online version of this paper and include the following:

- KEY RESOURCES TABLE
- RESOURCE AVAILABILITY
  - Lead contact
  - Materials availability
  - Data and code availability
- EXPERIMENTAL MODEL AND SUBJECT DETAILS
  - *Xenopus laevis* tadpoles
  - Microalgae *Chlamydomonas reinhardtii* wildtype and *Chlamydomonas reinhardtii* nac2-26 strain
  - Cyanobacteria *Synechocystis 6803* wildtype and Cyanobacteria *Synechocystis 6803 TD41* strain

SUPPLEMENTAL INFORMATION

Supplemental information can be found online at https://doi.org/10.1016/j.isci.2021.103158.

ACKNOWLEDGMENTS

The authors acknowledge financial support from the German Science Foundation (CRC 870; STR 478/3-1, KU 1282/9-1, TRR 175, NI390/9-2), the German Federal Ministry of Education and Research under the Grant code 01 EO 0901 and the Munich Center for Neuroscience.

AUTHOR CONTRIBUTIONS

Conceptualization: H.S., J.N., L.K.; Methodology: S.Ö., M.N.C., R.S., H.S.; Validation: S.Ö., H.S.; Formal analysis: S.Ö.; Investigation: S.Ö., M.N.C., R.S., H.S.; Resources: H.S., J.N. L.K.; Data curation: S.Ö.; Writing - original draft: S.Ö., H.S.; Writing - review & editing: S.Ö., H.S., L.K., J.N.; Visualization: S.Ö., H.S.; Supervision: H.S., J.N.; Project administration: H.S.; Funding acquisition: H.S., J.N.;

DECLARATIONS OF INTERESTS

The authors declare no competing or financial interests.

INCLUSION AND DIVERSITY

We worked to ensure sex balance in the selection of non-human subjects. We worked to ensure diversity in experimental samples through the selection of the cell lines.

ETHICS STATEMENT

All experiments were carried out in accordance with ARRIVE guidelines and regulations. Permission for these experiments was granted by the ethics committee for animal experimentation of the legally responsible governmental institution (Regierung von Oberbayern) under the license codes ROB-55.2.2532.Vet_03-17-24 and ROB-55.2.2532.Vet_02-19-128. In addition, all experimental methods were performed in accordance with the relevant guidelines and regulations of the Ludwig-Maximilians-University Munich.

Received: July 9, 2021
Revised: September 3, 2021
Accepted: September 17, 2021
Published: October 13, 2021

REFERENCES

Alvarez, M., Reynaert, N., Chávez, M.N., Aedo, G., Araya, F., Hopfner, U., Fernández, J., Allende, M.L., and Egaña, J.T. (2015). Generation of viable plant-vertebrate chimeras. PLoS One *10*, e0130295.

Ames, A. (2000). CNS energy metabolism as related to function. Brain Res. Rev. *34*, 42–68.

Bohne, A.-V., Schwarz, C., Schottkowski, M., Lidschreiber, M., Piotrowski, M., Zerges, W., and Nickelsen, J. (2013). Reciprocal regulation of protein synthesis and carbon metabolism for thylakoid membrane biogenesis. Plos Biol. *11*, e1001482. https://doi.org/10.1371/journal.pbio.1001482.

Boudreau, E., Nickelsen, J., Lemaire, S.D., Ossenbühl, F., and Rochaix, J.D. (2000). The Nac2 gene of Chlamydomonas encodes a chloroplast TPR-like protein involved in psbD mRNA stability. EMBO J. *19*, 3366–3376.

Burns, J.A., Kerney, R., and Duhamel, S. (2020). Heterotrophic carbon fixation in a salamander-alga symbiosis. Front. Microbiol. *11*, 1815.

Carreau, A., El Hafny-Rahbi, B., Matejuk, A., Grillon, C., and Kieda, C. (2011). Why is the partial oxygen pressure of human tissues a crucial parameter? Small molecules and hypoxia. J. Cell Mol. Med. *15*, 1239–1253.

Chávez, M.N., Schenck, T.L., Hopfner, U., Centeno-Cerdas, C., Somlai-Schweiger, I., Schwarz, C., Machens, H.G., Heikenwalder, M., Bono, M.R., Allende, M.L., et al. (2016). Towards autotrophic tissue engineering: photosynthetic gene therapy for regeneration. Biomaterials *75*, 25–36.

Chávez, M.N., Moellhoff, N., Schenck, T.L., Egaña, J.T., and Nickelsen, J. (2020). Photosymbiosis for biomedical applications. Front. Bioeng. Biotechnol. *8*, 577204.

Cobley, J.N., Fiorello, M.L., and Bailey, D.M. (2018). 13 reasons why the brain is susceptible to oxidative stress. Redox Biol. *15*, 490–503.

Cohen, J.E., Goldstone, A.B., Paulsen, M.J., Shudo, Y., Steele, A.N., Edwards, B.B., Patel, J.B., MacArthur, J.W., Jr., Hopkins, M.S., Burnett, C.E., et al. (2017). An innovative biologic system for photon-powered myocardium in the ischemic heart. Sci. Adv. *3*, e1603078.

Crystal, G.J., and Pagel, P.S. (2020). The physiology of oxygen transport by the cardiovascular system: evolution of knowledge. J. Cardiothorac. Vasc. Anesth. *34*, 1142–1151.

Fathollahipour, S., Patil, P.S., and Leipzig, N.D. (2018). Oxygen regulation in development: lessons from embryogenesis towards tissue engineering. Cells Tissues Organs *205*, 350–371.

Godwin, J.W., and Rosenthal, N. (2014). Scar-free wound healing and regeneration in amphibians: Immunological influences on regenerative success. Differentiation *87*, 66–75.

Hall, C.N., Klein-Flügge, M.C., Howarth, C., and Attwell, D. (2012). Oxidative phosphorylation, not glycolysis, powers presynaptic and postsynaptic mechanisms underlying brain information processing. J. Neurosci. *32*, 8940–8951.

Harris, E. (2008). The *Chlamydomonas* Sourcebook: Introduction to *Chlamydomonas* and its Laboratory Use, 2nd edn. (Elsevier).

Heinz, S., Rast, A., Shao, L., Gutu, A., Gügel, I.L., Heyno, E., Labs, M., Rengstl, B., Viola, S., Nowaczyk, M.M., et al. (2016). Thylakoid membrane architecture in *Synechocystis* depends on CurT, a homolog of the Granal CURVATURE THYLAKOID1 proteins. Plant Cell *28*, 2238–2260.

Hoiland, R.L., Howe, C.A., Coombs, G.B., and Ainslie, P.N. (2018). Ventilatory and cerebrovascular regulation and integration at high-altitude. Clin. Auton. Res. *28*, 423–435.

Hopfner, U., Schenck, T.L., Chávez, M.N., Machens, H.G., Bohne, A.V., Nickelsen, J., Giunta, R.E., and Egaña, J.T. (2014). Development of photosynthetic biomaterials for in vitro tissue engineering. Acta Biomater. *10*, 2712–2717.

Howarth, C., Gleeson, P., and Attwell, D. (2012). Updated energy budgets for neural computation in the neocortex and cerebellum. J. Cereb. Blood Flow Metab. *32*, 1222–1232.

Hyder, F., Rothman, D.L., and Bennett, M.R. (2013). Cortical energy demands of signaling and nonsignaling components in brain are conserved across mammalian species and activity levels. Proc. Natl. Acad. Sci. U. S. A. *110*, 3549–3554.

Kerney, R., Kim, E., Hangarter, R.P., Heiss, A.A., Bishop, C.D., and Hall, B.K. (2011). Intracellular invasion of green algae in a salamander host. Proc. Natl. Acad. Sci. U. S. A. *108*, 6497–6502.

Kooyman, G.L., McDonald, B.I., Williams, C.L., Meir, J.U., and Ponganis, P.J. (2020). The aerobic dive limit: after 40-years, still rarely measured but commonly used. Comp. Biochem. Physiol. A Mol. Integr. Physiol. *10*, 110841.

Lambert, F.M., Beck, J.C., Baker, R., and Straka, H. (2008). Semicircular canal size determines the developmental onset of angular vestibuloocular reflexes in larval *Xenopus*. J. Neurosci. *28*, 8086–8095.

Martin, W.F., Donald, A., Bryant, D.A., and Beatty, J.T. (2018). A physiological perspective on the origin and evolution of photosynthesis. FEMS Microbiol. Rev. *42*, 205–231.

Medzhitov, R. (2007). Recognition of microorganisms and activation of the immune response. Nature *449*, 819–826.

Neupert, J., Karcher, D., and Bock, R. (2009). Generation of *Chlamydomonas* strains that efficiently express nuclear transgenes. Plant J. *57*, 1140–1150.

Nieuwkoop, P.D., and Faber, J. (1994). Normal Table of *Xenopus laevis* (Daudin): A Systematical and Chronological Survey of the Development from the Fertilized Egg till the End of Metamorphosis (Garland).

Nixon, P.J., Trost, J.T., and Diner, B.A. (1992). Role of the carboxy terminus of polypeptide D1 in the assembly of a functional water-oxidizing manganese cluster in photosystem II of the cyanobacterium Synechocystis sp. PCC 6803: assembly requires a free carboxyl group at C-terminal position 344. Biochemistry *31*, 10859–10871.

Özugur, S., Kunz, L., and Straka, H. (2020). Relationship between oxygen consumption and neuronal activity in a defined neural circuit. BMC Biol. *18*, 76.

Piiper, J. (1982). Respiratory gas exchange at lungs, gills and tissues: mechanisms and adjustments. J. Exp. Biol. *100*, 5–22.

Poli, S., and Veltkamp, R. (2009). Oxygen therapy in acute ischemic stroke - experimental efficacy and molecular mechanisms. Curr. Mol. Med. *9*, 227–241.

Rippka, R., Deruelles, J., Waterbury, J.B., Herdman, M., and Stanier, R.Y. (1979). Generic assignments, strain histories and properties of pure cultures of cyanobacteria. Microbiology *111*, 1–61.

Sacca, R., and Burggren, W. (1982). Oxygen uptake in air and water in the air-breathing reedfish *Calamoichthys calabaricus*: role of skin, gills and lungs. J. Exp. Biol. *97*, 179–186.

Schenck, T.L., Hopfner, U., Chávez, M.N., Machens, H.G., Somlai-Schweiger, I., Giunta, R.E., Bohne, A.V., Nickelsen, J., Allende, M.L., and Egaña, J.T. (2015). Photosynthetic biomaterials: a pathway towards autotrophic tissue engineering. Acta Biomater. *15*, 39–47.

Schneider, J., Berndt, N., Papageorgiou, I.E., Maurer, J., Bulik, S., Both, M., Draguhn, A., Holzhütter, H.G., and Kann, O. (2019). Local oxygen homeostasis during various neuronal network activity states in the mouse hippocampus. J. Cereb. Blood Flow Metab. *39*, 859–873.

Soupiadou, P., Branoner, F., and Straka, H. (2018). Pharmacological profile of vestibular inhibitory inputs to superior oblique motoneurons. J. Neurol. *265*, S18–S25.

Straka, H., and Simmers, J. (2012). *Xenopus laevis*: an ideal experimental model for studying the developmental dynamics of neural assembly and sensory motor computations. Dev. Neurobiol. *72*, 649–663.

Venn, A.A., Loram, J.E., and Douglas, A.E. (2008). Photosynthetic symbioses in animals. J. Exp. Bot. *59*, 1069–1080.

West, J.B. (2018). A lifetime of pulmonary gas exchange. Physiol. Rep. *6*, e13903.

STAR★METHODS

KEY RESOURCES TABLE

REAGENT or RESOURCE	SOURCE	IDENTIFIER
Chemicals, peptides, and recombinant proteins		
Tris acetate phosphate growth medium	Nickelsen laboratory, Department Biology I, Ludwig-Maximilians-University Munich, Faculty of Biology, Ludwig-Maximilians-University Munich	Bohne et al. (2013)
BG11 growth medium	Nickelsen laboratory, Department Biology I, Ludwig-Maximilians-University Munich, Faculty of Biology, Ludwig-Maximilians-University Munich	Heinz et al. (2016)
Sorbitol	Carl Roth, Germany	Cat# 6213.1
3-aminobenzoic acid ethyl ester methanesulfonate (MS-222	Pharmaq Ltd. UK	N/A
NaCl	Carl Roth, Germany	Cat# 3957.3
$NaCO_3$	Carl Roth, Germany	Cat# 8551.1
KCl	Carl Roth, Germany	Cat# P017.1
Glucose monohydrate	Carl Roth, Germany	Cat# 6780.1
$CaCl_2$	Carl Roth, Germany	Cat# T885.2
$MgCl_2$	Carl Roth, Germany	Cat# 2189.1
Isolectin GS-IB4, Alexa Fluor 488 Conjugate	Invitrogen (Thermo Fisher Scientific)	Cat# I21411
Paraformaldehyde	Carl Roth, Germany	Cat# 0335.3
L-Ascorbic acid	Sigma Life Science (Merck)	Cat# A4544-25G
NaOH	Carl Roth, Germany	Cat# 6771
Hepes	Carl Roth, Germany	Cat# 9105.2
Sorbitol	Carl Roth, Germany	Cat# 6213.2
Chloramphenicol	Carl Roth, Germany	Cat# 3886.2
Experimental models: Organisms/strains		
Xenopus laevis wildtype	Institutional breeding facility, Faculty of Biology, Ludwig-Maximilians-University Munich	N/A
Chlamydomonas reinhardtii wildtype	Department Biology I, Ludwig-Maximilians-University Munich, Faculty of Biology, Ludwig-Maximilians-University Munich	Neupert et al. (2009)
Chlamydomonas reinhardtii nac2-26 strain	Department Biology I, Ludwig-Maximilians-University Munich, Faculty of Biology, Ludwig-Maximilians-University Munich	Boudreau et al. (2000)
Cyanobacteria *Synechocystis* 6803 wildtype	Department Biology I, Ludwig-Maximilians-University Munich, Faculty of Biology, Ludwig-Maximilians-University Munich	NA
Cyanobacteria *Synechocystis* 6803 TD41 strain	Department Biology I, Ludwig-Maximilians-University Munich, Faculty of Biology, Ludwig-Maximilians-University Munich	Nixon et al. (1992)

(*Continued on next page*)

Continued

REAGENT or RESOURCE	SOURCE	IDENTIFIER
Software and algorithms		
ZEN Imaging software (blue edition) 3.0	ZEISS, Germany	N/A
Data recording and analysis: Spike 2 version 7.04	Cambridge Electric Design Limited (CED), UK	N/A
Data analysis: Microcal Origin 6.0G	OriginLab Corp., USA	N/A
Statistical tests: Prism version	Graphpad Software, LLC, Inc, USA	N/A
Figure assembly: Affinity Designer 1.8.3	Serif Europe, UK	N/A

RESOURCE AVAILABILITY

Lead contact

- Further information and requests for resources and reagents should be directed to and will be fulfilled by the lead contact, Dr. Hans Straka (straka@lmu.de).

Materials availability

- This study did not generate new unique reagents.

Data and code availability

- All data reported in this paper will be shared by the lead contact upon request.
- This paper does not report original code.
- Any additional information required to reanalyze the data reported in this paper is available from the lead contact upon request.

EXPERIMENTAL MODEL AND SUBJECT DETAILS

Xenopus laevis tadpoles

Wildtype *Xenopus laevis* tadpoles of either sex (n = 94) at developmental stages 52-53 (Nieuwkoop and Faber, 1994) were obtained from the in-house animal breeding facility at the Biocenter-Martinsried of the Ludwig-Maximilians-University Munich. Embryos were obtained following manual collection of the eggs after natural mating. Embryos were allowed to grow in standing tanks of de-chlorinated water at 17-19°C under a 12 hr/12 hr light/dark cycle, and were fed daily with a powdered Spirulina (Algova, Germany) suspension in tank water until use for experimentation at stages 52-53. All experiments were carried out in accordance with ARRIVE guidelines and regulations. Permission for these experiments was granted by the ethics committee for animal experimentation of the legally responsible governmental institution (Regierung von Oberbayern) under the license codes ROB-55.2.2532.Vet_03-17-24 and ROB-55.2.2532.Vet_02-19-128. In addition, all experimental methods were performed in accordance with the relevant guidelines and regulations of the Ludwig-Maximilians-University Munich.

Microalgae *Chlamydomonas reinhardtii* wildtype and *Chlamydomonas reinhardtii* nac2-26 strain

The cell-wall deficient, arginine phototropic, *cw15*-30-derived UVM11 *C. reinhardtii* strain (Neupert et al., 2009) and the photomutant *nac2-26* strain of *C. reinhardtii* (Boudreau et al., 2000) were grown photomixotrophically at room temperature on Tris acetate phosphate (TAP)-agar plates at continuous light (30 μE) (Bohne et al., 2013). Microalgae cultures were streaked into fresh plates once a month to maintain a healthy color and growth capacity. Liquid precultures were prepared by inoculating solid microalgae colonies in TAPS (TAP-medium supplemented with 1% weight/volume sorbitol) medium supplemented with 1% (w/v) sorbitol (TAPS) and chloramphenicol (10 μg/mL) under standard culture conditions (23°C, constant illumination at 30 $\mu E \cdot m^{-2} \cdot s^{-1}$ and agitation at 120 rpm). TAP medium was prepared as described in the literature (Harris, 2008). For the preparation of the algae, the preculture was transferred into 1-liter medium and incubated for 4 - 5 days to reach a final cell-concentration of 1 x 10^7 cells/ml. All algae cultures were used at middle log-phase to prevent the accumulation of cell debris. Cell numbers were determined under a microscope using a Neubauer-chamber. The appropriate culture-volume was centrifuged at room

temperature (5 min, 1200 rpm) and cells were resuspended in frog Ringer solution (details see below) at a concentration of 10 x 10^9 cells/ml. Cell-culture manipulations were performed under laminar flow and sterile conditions.

Cyanobacteria *Synechocystis 6803* wildtype and Cyanobacteria *Synechocystis 6803 TD41* strain

The wild-type cyanobacteria *Synechocystis* 6803 strain and its photomutant *TD41* (Nixon et al., 1992) were kept on BG11-medium agar-plates supplemented with 5 mM glucose at 28°C (Heinz et al., 2016) and under constant illumination (30 μE, white light) according to the literature (Rippka et al., 1979). Cyanobacteria were streaked onto fresh plates once a month to maintain the colonies in good health. The *TD41* strain lacks the three copies of the *psbA* gene encoding the photosystem II subunit D1, thus rendering it incapable of photosynthetic oxygen production (Nixon et al., 1992). Liquid precultures were started from agar-growing colonies in 50 ml BG11-medium supplemented with glucose and used for inoculation of 0.75-liter cultures at an OD750 = 0.01 (eq. $2 \cdot 10^5$ cells x ml^{-1}). Cultures were kept in a custom-made bioreactor with constant aeration and illumination (28°C, 30 μE) for 3-4 days until an OD750 ≥ 2 (middle log-phase) was reached. Cyanobacteria were brought to the required cell-density by centrifugation at room temperature (5 min, 3000 g) and subsequent resuspension in frog Ringer solution (see below). Cell-culture manipulations were performed under laminar flow and sterile conditions.

METHOD DETAILS

Determination of oxygen production in isolated algae

To evaluate the O_2 production capacity of isolated *C. reinhardtii* and *Synechocystis* 6803, 5 × 10^8 cells/ml and 10^8 cells/ml, respectively, were suspended in 5 ml frog Ringer solution and prepared for monitoring the O_2 concentration with electrochemically sensitive electrodes (see below). A light source (Zeiss CL 6000 LED, with > 150 W, 600 lm) was placed at a distance of 5 cm from the samples. The light intensity was set to 100 μE. Throughout the measurements, the ambient temperature was kept constant at 17°C in a temperature-controlled box.

Injection of algal suspension

Xenopus tadpoles were deeply anesthetized in 0.05% 3-aminobenzoic acid ethyl ester methanesulfonate (MS-222; Pharmaq Ltd. UK) in ice-cold frog Ringer solution (in mol/L: 75 NaCl, 25 $NaHCO_3$, 2 $CaCl_2$, 2 KCl, 0.5 $MgCl_2$, 11 glucose, and 0.01 Hepes, pH 7.4), mechanically secured ventral side up with U-shaped pins in a Sylgard-lined dish of 5 cm diameter and maintained in chilled MS-222 Ringer solution (0.05%) throughout the injection procedure. Prior to the trans-cardial injection, the skin above the heart was gently removed. Glass capillaries for the injection of the algal suspensions were pulled on a P-87 Brown/Flaming electrode puller from borosilicate glass (Science Products, Hofheim, Germany), broken and beveled to a tip diameter of 20 - 30 μm and a tip angle of 30°. Glass capillaries were filled with a total volume of 10 μl algal suspension (*C. reinhardtii* or *Synechocystis* 6803) at a concentration of 10 x 10^9 cells/ml, dissolved in oxygenated (carbogen 95% O_2, 5% CO_2) frog Ringer (see above). The injection electrode was inserted into an electrode holder connected to a pressure application system and mounted onto a 3-axes-micromanipulator (Bachofer, Reutlingen, Germany).

The tip of the glass capillary, filled with the solution of suspended *C. reinhardtii*, *Synechocystis* 6803, or their respective photomutants, was directly placed above the heart and the position of the tip was manually adjusted with the micro-manipulator to allow an insertion of the injection electrode into the ventricular chamber of the heart (Figure 1D). Once placed firmly inside the heart, the algal suspension was pressure-injected by single pulses with a duration of 100 - 200 ms (Pulse master A300; World Precision Instruments, Sarasota, USA), produced by a pressure injector (PDES-02T; npi Electronics, Tamm, Germany) at a magnitude of 1 - 2 bar. Each pulse corresponded to an approximately injected volume of 0.1 – 0.2 μl. The pulses were triggered manually according to the rhythm of the heart beat and were applied over a period of ∼30 min at a rate of ∼2 - 3 pulses/min (maximal injected volume: 10 μl). This allowed the algae to spread throughout the vascular system, verified as gradually increasing green staining of blood vessels, in particular those within the skin (Figures 1E and 1F). After slowly retracting the injection electrode, the deeply anesthetized tadpoles were prepared for the subsequent isolation of the tissue.

Visualization of algae within the vascular system

A volume of 2 μl Isolectin (200 nM, coupled to Alexa Fluor 488, Thermofisher; Germany) was injected together with 8 μl of a suspension of *C. reinhardtii* or *Synechocystis* 6803 in frog Ringer at a concentration of 10 x 10^9 cells/ml. This mixture was used to visualize blood vessels through a binding to the Isolectin oligosaccharide component to the endothelial wall of the vessels. Following immediate decapitation after the injection, the tissue was fixated in 4% paraformaldehyde for 8 hours. Thereafter, the tissue was cleared in glycerol and prepared for confocal microscopy. Whole brains were imaged on a Zeiss LSM 900-Airyscan-2 microscope with a 10x objective using the software ZEN (blue edition) 3.0 and were reconstructed by sequences (z-stack) of 445 optical sections at a thickness of 1.33 μm (Figure S1A and Video S2 for the z-stack of the entire brain). Detailed images of individual blood vessels, filled with *Synechocystis* 6803, were obtained with a Zeiss LSM 900-Airyscan-2 microscope using a 20x objective and the ZEN (blue edition) 3.0 software. The 71.6 μm thick portion of the tissue was imaged by optical sectioning at 0.39 μm (Figure 1H). Using a 40x objective and 58.8 μm thick portion of tissue and optical sectioning at 0.21 μm resulted in detailed images of single blood vessels (Figures 1J and S1B1–S1B3). Tissue containing *C. reinhardtii* was imaged using a Mavig VivaScope RS-G4, 60x Olympus (UPLSAPO60XO, NA 1.3) oil objective, with 95 μm thickness of the imaged volume sample, and 1.5 μm optical sections (Figures 1G, 1I and S1C). The excitation wavelength of chlorophyll in the algae was 655/640 nm (green), and for Isolectin 493/488 nm (red) for the Zeiss LSM 900-Airyscan-2 and the VivaScope RS-G4 microscope, respectively.

Isolation of the whole head preparation

Deeply anesthetized *Xenopus* tadpoles, injected prior with the algal suspension were decapitated at the level of the upper spinal cord and eviscerated. The skin above the head was partially removed, the skull opened, the forebrain disconnected and both optic nerves severed. If not stated otherwise, the choroid plexus above the IV^{th} ventricle remained in place. The residual central nervous system with efferent and afferent connections to persisting sensory organs and motor effectors remained functionally preserved (Straka and Simmers, 2012). In part of the experiments, multi-unit spike discharge was recorded from the *superior oblique* motor nerve after disconnection from the target muscle at the innervation site. Following completion of the isolation process, preparations were allowed to recover for ~2 hours at 17°C in darkness before commencing with the recording session. For all experiments, isolated preparations were placed in a Sylgard-lined recording chamber that was continuously superfused with a Ringer solution at a constant temperature of 17.0 ± 0.5°C. The Ringer volume of the bath chamber was ~2 ml with ~3 mm of Ringer above the dorsal surface of the isolated preparation. The oxygen concentration of the bath Ringer under control conditions was air-saturated (~270 μmol/L) and was experimentally increased up to ~1100 μM and decreased to ~40 μmol/L by ventilation with carbogen (95% O_2, 5% CO_2) and nitrogen (N_2), respectively as described previously (Özugur et al., 2020). The ventilation of the Ringer solution was performed in a separate ante-chamber (2 ml volume) with a rapid outflow into the recording chamber. The isolated preparation was generally maintained in darkness in order to prevent photosynthesis of the microorganisms. To illuminate the photosynthetic microorganisms inside the brain vascular system, a light source (Zeiss CL 6000 LED, with > 150 W, 600 lm), placed at a distance of 5 cm from the isolated preparations, was targeted onto the brain. The light intensity was set to 100 μE.

Recordings of oxygen dynamics and neuronal activity

The O_2 concentration of the Ringer solution in the bath and the IV^{th} ventricle between the caudal end of the cerebellum and the rostral end of the choroid plexus was continuously monitored by O_2-sensitive electrodes (Unisense A/S, Denmark) with tip diameters of 10 μm. Measurements of the oxygen level at this position within the IV^{th} ventricle has previously been shown to directly represent the O_2 level of the adjacent hindbrain with the advantage that the brain tissue remains unimpaired (Özugur et al., 2020). Electrodes were freshly calibrated prior to each experiment using a solution with 0 μmol/L oxygen (0.1 mol/L ascorbic acid in 0.1 mol/L NaOH), 270 μmol/L oxygen (air saturated Ringer solution), and 1350 μmol/L oxygen (carbogen saturated Ringer solution), temperature adjusted to 17°C. O_2 electrodes were positioned and advanced with a piezo-stepper (Sensapex, Finland) attached to a micromanipulator (Sensapex, Finland). The spontaneous spike discharge of the *superior oblique* motor nerve as a proxy for central nervous activity was recorded extracellularly (EXT 10-2F; npi electronics; Tamm, Germany) with glass suction electrodes (Özugur et al., 2020). Electrodes were pulled on a P-87 Brown/Flaming electrode puller from borosilicate glass (Science Products, Hofheim, Germany) and individually broken to fit the diameter of the recorded nerve. O_2 concentrations and concurrent spike activity were digitized at 120 Hz and 5 kHz, respectively (CED 1401, Cambridge Electronic Design, UK) and stored on computer for offline analysis.

QUANTIFICATION AND STATISTICAL ANALYSIS

Discharge rates of the *superior oblique* motor nerve were obtained from multi-unit spike activity using Spike2 (Cambridge Electronic Design, UK) scripts. Spike rates derived from spike times in a given recording by counting all events above an amplitude threshold that was set to ~1.5x of the amplitude of the noise level and remained unaltered for a given experiment (Özugur et al., 2020). Under air-saturated control O_2 concentrations, the multi-unit resting rate ranged from 30-50 spikes/s in different preparations (Soupiadou et al., 2018). The spike events were plotted as discharge rates with a bin width of 1 s. O_2 concentrations in the IV^{th} ventricle and bath chamber were continuously measured as described above and recorded together with the neuronal activity.

All analysis steps were performed in Spike2 and/or in Microcal Origin 6.0G (OriginLab Corp., USA) using implemented standard algorithms for the different computations. Data plotting was performed in Microcal Origin 6.0G. Data are presented as dot and whisker box plots and values are indicated as mean ± sem, if not stated otherwise. Statistical differences between experimental groups were calculated with the non-parametric Mann-Whitney *U*-test (unpaired parameters) or the Wilcoxon signed-rank test (paired parameters; Prism, Graphpad Software, Inc, USA) with Bonferroni corrections in the case of multiple comparisons and indicated as *p*-values (* $p < 0.05$; ** $p < 0.001$; *** $p < 0.0001$).